NASA/TM—2003-212113

AIAA–2003–1300

Measurements of Shear Lift Force on a Bubble in Channel Flow in Microgravity

Henry K. Nahra and Brian J. Motil
Glenn Research Center, Cleveland, Ohio

Mark Skor
Baldwin Wallace College, Berea, Ohio

January 2003

The NASA STI Program Office . . . in Profile

Since its founding, NASA has been dedicated to the advancement of aeronautics and space science. The NASA Scientific and Technical Information (STI) Program Office plays a key part in helping NASA maintain this important role.

The NASA STI Program Office is operated by Langley Research Center, the Lead Center for NASA's scientific and technical information. The NASA STI Program Office provides access to the NASA STI Database, the largest collection of aeronautical and space science STI in the world. The Program Office is also NASA's institutional mechanism for disseminating the results of its research and development activities. These results are published by NASA in the NASA STI Report Series, which includes the following report types:

- TECHNICAL PUBLICATION. Reports of completed research or a major significant phase of research that present the results of NASA programs and include extensive data or theoretical analysis. Includes compilations of significant scientific and technical data and information deemed to be of continuing reference value. NASA's counterpart of peer-reviewed formal professional papers but has less stringent limitations on manuscript length and extent of graphic presentations.

- TECHNICAL MEMORANDUM. Scientific and technical findings that are preliminary or of specialized interest, e.g., quick release reports, working papers, and bibliographies that contain minimal annotation. Does not contain extensive analysis.

- CONTRACTOR REPORT. Scientific and technical findings by NASA-sponsored contractors and grantees.

- CONFERENCE PUBLICATION. Collected papers from scientific and technical conferences, symposia, seminars, or other meetings sponsored or cosponsored by NASA.

- SPECIAL PUBLICATION. Scientific, technical, or historical information from NASA programs, projects, and missions, often concerned with subjects having substantial public interest.

- TECHNICAL TRANSLATION. English-language translations of foreign scientific and technical material pertinent to NASA's mission.

Specialized services that complement the STI Program Office's diverse offerings include creating custom thesauri, building customized databases, organizing and publishing research results . . . even providing videos.

For more information about the NASA STI Program Office, see the following:

- Access the NASA STI Program Home Page at ***http://www.sti.nasa.gov***

- E-mail your question via the Internet to help@sti.nasa.gov

- Fax your question to the NASA Access Help Desk at 301–621–0134

- Telephone the NASA Access Help Desk at 301–621–0390

- Write to:
  NASA Access Help Desk
  NASA Center for AeroSpace Information
  7121 Standard Drive
  Hanover, MD 21076

NASA/TM—2003-212113 AIAA–2003–1300

Measurements of Shear Lift Force on a Bubble in Channel Flow in Microgravity

Henry K. Nahra and Brian J. Motil
Glenn Research Center, Cleveland, Ohio

Mark Skor
Baldwin Wallace College, Berea, Ohio

Prepared for the
41st Aerospace Sciences Meeting and Exhibit
sponsored by the American Institute of Aeronautics and Astronautics
Reno, Nevada, January 6–9, 2003

National Aeronautics and
Space Administration

Glenn Research Center

January 2003

Acknowledgments

The authors wish to thank the NASA Glenn Research Center's Microgravity Fluid Physics Branch for the support provided to accomplish this work.

Available from

NASA Center for Aerospace Information
7121 Standard Drive
Hanover, MD 21076

National Technical Information Service
5285 Port Royal Road
Springfield, VA 22100

Available electronically at http://gltrs.grc.nasa.gov

REPORT DOCUMENTATION PAGE

Form Approved
OMB No. 0704-0188

1. AGENCY USE ONLY (*Leave blank*)	2. REPORT DATE	3. REPORT TYPE AND DATES COVERED
	January 2003	Technical Memorandum

4. TITLE AND SUBTITLE

Measurements of Shear Lift Force on a Bubble in Channel Flow in Microgravity

5. FUNDING NUMBERS

WBS–22–101–53–01

6. AUTHOR(S)

Henry K. Nahra, Brian J. Motil, and Mark Skor

7. PERFORMING ORGANIZATION NAME(S) AND ADDRESS(ES)

National Aeronautics and Space Administration
John H. Glenn Research Center at Lewis Field
Cleveland, Ohio 44135–3191

8. PERFORMING ORGANIZATION REPORT NUMBER

E–13756

9. SPONSORING/MONITORING AGENCY NAME(S) AND ADDRESS(ES)

National Aeronautics and Space Administration
Washington, DC 20546–0001

10. SPONSORING/MONITORING AGENCY REPORT NUMBER

NASA TM—2003-212113
AIAA–2003–1300

11. SUPPLEMENTARY NOTES

Prepared for the 41st Aerospace Sciences Meeting and Exhibit sponsored by the American Institute of Aeronautics and Astronautics, Reno, Nevada, January 6–9, 2003. Henry K. Nahra and Brian J. Motil, NASA Glenn Research Center; Mark Skor, Baldwin Wallace College, Berea, Ohio 44017. Responsible person, Henry K. Nahra, organization code 6712, 216–433–5385.

12a. DISTRIBUTION/AVAILABILITY STATEMENT

Unclassified - Unlimited
Subject Category: 34 Distribution: Nonstandard

Available electronically at http://gltrs.grc.nasa.gov

This publication is available from the NASA Center for AeroSpace Information, 301–621–0390.

12b. DISTRIBUTION CODE

13. ABSTRACT ***(Maximum 200 words)***

Under microgravity conditions, the shear lift force acting on bubbles, droplets or solid particles in multiphase flows becomes important because under normal gravity, this hydrodynamic force is masked by buoyancy. This force plays an important role in furnishing the detachment process of bubbles in a setting where a bubble suspension is needed in microgravity. In this work, measurements of the shear lift force acting on a bubble in channel flow are performed. The shear lift force is deduced from the bubble kinematics using scaling and then compared with predictions from models in literature that address different asymptotic and numerical solutions. Basic trajectory calculations are then performed and the results are compared with experimental data of position of the bubble in the channel. A direct comparison of the lateral velocity of the bubbles is also made with the lateral velocity prediction from investigators, whose work addressed the shear lift on a sphere in different two-dimensional shear flows including Poiseuille flow.

14. SUBJECT TERMS

Shear lift; Drag; Bubble; Detachment; Microgravity

15. NUMBER OF PAGES

17

16. PRICE CODE

17. SECURITY CLASSIFICATION OF REPORT	18. SECURITY CLASSIFICATION OF THIS PAGE	19. SECURITY CLASSIFICATION OF ABSTRACT	20. LIMITATION OF ABSTRACT
Unclassified	Unclassified	Unclassified	

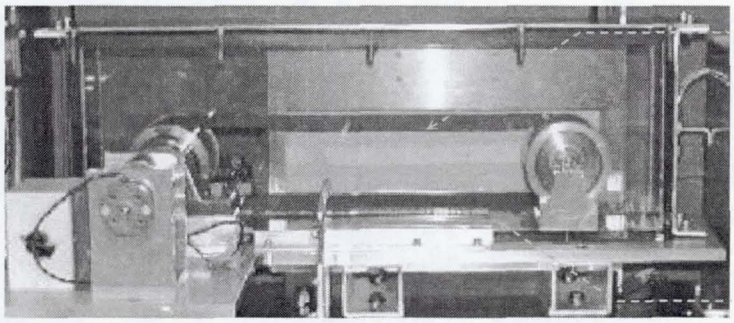

Figure 10. Simple shear flow apparatus integrated in the Multiphase Flow Rig (MFR).

REFERENCES

Auton, T.R. "The Lift Force on a Spherical Body in a Rotational Flow," *J. Fluid Mech.,* **183,** 199–218, (1987).

Cherukat, P.; McLaughlin, J.B.; and Graham, A.L. "The Inertial Lift on a Rigid Sphere Translating in a Linear Shear Flow Field," *Int. J. Multiphase Flow*, **20**, No. 2, 339–353, (1994).

Cherukat, P.; and McLaughlin, J.B. "Wall-induced Lift on a Rigid Sphere," *Int. J. Multiphase Flow*, **16**, No. 2, pp. 899–907, (1990).

Cox, R.G.; and Brenner, H. "The Lateral Migration of Solid Particles in Poseuille Flow: I. Theory," *Chem. Engng. Sci.* **23**, 147–173, (1968).

Dandy, D.S.; and Dwyer, H.A. "A Sphere in Shear Flow at Finite Reynolds Number: Effect of Shear on Particle lift, Drag, and Heat Transfer," *J. Fluid Mech.,* **216,** 381–410, (1990).

Kariyasaki, A. "Behavior of a Single Gas Bubble in a Liquid Flow With a Linear Velocity Profile," *Proc. 1987 ASME-JSME Thermal Engineering Joint Conference*, ASME, New York, p. 261, (1987).

Legendre, D.; and Magnaudet, J. "The Lift Force on a Spherical Bubble in a Viscous Linear Shear Flow," *J. Fluid Mech.,* **368,** 81–126, (1998).

Leighton, D.T.; and Acrivos, A. "The Lift on a Small Sphere Touching a Plane in the Presence of a Simple Shear Flow," *Z. Agnew. Math. Phys.* **36**, 174–178, (1985).

McLaughlin, J.B. "Inertial Migration of Small Sphere in Linear Shear Flows," *J. Fluid Mech.,* **224,** 261–274, (1991).

Rubinow, S.I.; Keller, J.B. "The Transverse Force on a Spinning Sphere Moving in a Viscous Fluid," *J. Fluid Mech.,* **11**, 447–459, (1961).

Saffman, P.G. "The Lift on a Small Sphere in a Slow Shear Flow," *J. Fluid Mech,* **22**, Part 2, 385–400, (1965).

Takemura, F.; Takagi, S.; Magnaudet, J.; and Matsumoto, Y. "Drag and Lift Forces on a Bubble Rising near a Vertical Wall in a Viscous Liquid," *J. Fluid Mech.,* **461**, 277–300, (2002).

Vasseur, P.; and Cox, R.G. "The Lateral Migration of a Spherical Particle in Two-dimensional Shear Flows," *J. Fluid Mech.*, **78**, Part 2, 385–413, (1976).

MEASUREMENTS OF SHEAR LIFT FORCE ON A BUBBLE IN CHANNEL FLOW IN MICROGRAVITY

Henry K. Nahra* and Brian J. Motil†
National Aeronautics and Space Administration
Glenn Research Center
Cleveland, Ohio 44135
Henry.K.Nahra@grc.nasa.gov
Brian.J.Motil@grc.nasa.gov

Mark Skor
Baldwin-Wallace College
Berea, Ohio 44017
maskor@bw.edu

ABSTRACT

Under microgravity conditions, the shear lift force acting on bubbles, droplets or solid particles in multiphase flows becomes important because under normal gravity, this hydrodynamic force is masked by buoyancy. This force plays an important role in furnishing the detachment process of bubbles in a setting where a bubble suspension is needed in microgravity. In this work, measurements of the shear lift force acting on a bubble in channel flow are performed. The shear lift force is deduced from the bubble kinematics using scaling and then compared with predictions from models in literature that address different asymptotic and numerical solutions. Basic trajectory calculations are then performed and the results are compared with experimental data of position of the bubble in the channel. A direct comparison of the lateral velocity of the bubbles is also made with the lateral velocity prediction from Vasseur and Cox (1976) whose work addressed the shear lift on a sphere in different two-dimensional shear flows including Poiseuille flow.

INTRODUCTION AND LITERATURE REVIEW

Understanding of the shear lift force acting on a bubble, droplet or solid sphere is crucial to understanding the behavior of bubbly flows; bubble segregation in bubble suspensions; droplet coalescence and segregation; and particle sedimentation. Lateral motion of bubbles/particles due to shear flow could result in bubble segregation, which in turn results in impacts on the efficiency of heat and mass transfer processes such as liquid-gas phase separation and phase contacting in bioreactors. An understanding of the shear lift force results in a more accurate closure law to incorporate in two-phase flow modeling as applicable to nuclear space power.

Literature Review

Several investigators have addressed the shear lift force analytically under different flow regimes. Rubinow and Keller (1961) addressed the problem of a sphere that translates and rotates in a still fluid and solved for the flow field using an asymptotic matching techniques of the near and far (inner and outer) regions. They calculated the shear lift to be dependent on the sphere radius, the liquid density and the translation and angular velocities, i.e. $\boldsymbol{F}_L = \pi a^3 \rho \boldsymbol{\Omega} \times \boldsymbol{V}(1 + O(Re_p))$. Saffman (1965) calculated the shear lift force acting on a sphere in a simple shear flow using asymptotic matching. His assumptions were that the Reynolds numbers based on the liquid velocity, the shear rate, and the angular velocity were small, and the shear rates were high. McLaughlin (1991, 1993) revisited the calculation by Saffman and relaxed the condition on the high shear rates. Vasseur and Cox (1976) solved the inner region problem by assuming that the wall falls within the influence of the inner region, and by that the sphere diameter is very small such that the disturbance by the flow can be taken as caused by a point force. They calculated the migration velocity due to shear lift for a neutrally buoyant and non-buoyant sphere in a still liquid, simple shear and Poiseuille like flow. Leighton and Acrivos (1985) calculated the shear lift on a particle tangent to the wall in a shear flow. The aforementioned contributions were for a low Reynolds number that is based on the characteristic velocity and particle diameter. For flows of high

*AIAA Associate Fellow, 2003
† AIAA Member

Reynolds numbers, Auton (1987) calculated the shear lift by solving the inviscid vorticity problem with low shear rate and calculating the longitudinal component of velocity perturbation. Using Bernouilli's equation, the pressure distribution and thereafter the shear lift were calculated. For intermediate Reynolds numbers, two contributions are cited. Dandy and Dwyer, (1990) performed a 3-D numerical calculation for steady linear shear flow past a heated spherical particle over a wide range of Re, $0.1 < Re < 100$ and dimensionless shear rate Sr, $0.005 < Sr < 0.4$. They found that the lift coefficient $C_L \sim Re^{-1/2}$ at low Re and constant C_L over a wide range of Re at a fixed Sr. Lift contribution from pressure and viscous forces were calculated. Legendre and Magnaudet (1998) performed a 3-D numerical calculation for a bubble fixed in a simple shear flow field. They solved the full Navier-Stokes and continuity equations for $0.1 < Re < 500$ and $Sr < 1$. They studied the tangential velocity on the bubble surface, and the effect of Re on streamwise vorticity. They found that at low Re, C_L depended on Sr and Re, and for moderate to high Re such a dependence was found to be very weak.

Investigators measured the shear lift force on spheres and bubbles as well under normal gravity conditions. Kariyasaki (1987) measured the shear lift on bubbles, spheres and droplets in a simple shear flow and compared his results with predictions from Rubinow and Keller's (R-B) and Saffman's models. A shear lift expression was also derived in his work that reflected the significant deformation of bubble shape in the shear flow. With this shear model at hand, Kariyasaki calculated the bubble trajectories and compared with his experimental data. Cherukat and McLaughlin (1990) studied the lateral migration of rigid spheres sedimenting near a large flat wall in a quiescent Newtonian fluid for $0.1 < Re < 10$. Comparison of experimental results with prediction showed that the expression derived by Vasseur and Cox (1977) predicted fairly well the migration velocity up to $Re \sim 3$. Cherukat, McLaughlin, and Graham (1994) studied the shear induced inertial migration of rigid spheres experimentally in a simple shear flow established by a shear flow apparatus. They measured the migration velocity, which compared well with Saffman's and McLaughlin's predictions for $0.1 < Re < 2.5$. Takemura *et al.* (2002) determined experimentally the two components of drag and lift acting on a clean almost spherical bubble rising near a plane vertical wall in a quiescent liquid up to $Re \sim 40$. They found the existence of two regimes according to the dimensionless separation L^* defined as the ratio between the distance from the bubble center to the wall d and the viscous length ν/U, i.e. $L^* = d/(\nu/U)$. For $L^* \sim O(1)$ or more and for $Re < 1$, results were found to be in good agreement with an analytical solution obtained in the Oseen approximation by adapting the calculation of Vasseur and Cox (1977) to the case of an inviscid bubble. When $L^* \sim o(1)$, measurements have shown that the bubble deformation was significant when the viscosity of the surrounding liquid is large enough. This deformation may be attributed to the fact that higher order effects, not taken into consideration in the aforementioned calculation became important.

The interest of this work lies in the measurement of the shear lift force based on the bubble kinematics under microgravity conditions. The microgravity environment eliminates the buoyancy force and thereby the possibility of bubble deformation, which if present, introduces another source for lift that is associated with the bubble shape. This presents a technical difficulty in separating the two sources of lift.

Measurement of the shear lift force on a bubble of intermediate diameter range (2 to 5 mm) under normal gravity conditions and using bubble kinematics is rather difficult because of the inherent deformation experienced by the bubble. Generation of spherical bubbles (2 to 5 mm) under normal gravity is rather difficult. The range of bubble Reynolds number is governed under normal gravity by the bubble terminal velocity $U_t \sim 20$ to 30 cm/s. Therefore, the interest in making microgravity measurements of the shear lift force acting on a bubble in a shear flow motivated this study.

ORIGIN OF SHEAR LIFT

The shear lift force on a bubble is attributed as described by Legendre and Magnaudet (1998) to the secondary velocity field at the surface of the bubble. V_ϕ is a crucial quantity since the lift comes from the fact that the pressure and normal viscous stresses have a non-constant azimuthal distribution. Here V_ϕ, following a spherical coordinate system, is defined as $V_\phi(\theta,\phi) = \boldsymbol{V}(r = R, \theta,\phi)\bullet\boldsymbol{e}_\phi$ lying in the plane $\theta =$ constant normal to the unperturbed flow. Since $\boldsymbol{U}_L\bullet\boldsymbol{e}_\phi = 0$ far away from the bubble, this V_ϕ component is a secondary velocity that does not directly result from the unperturbed flow. At low Reynolds numbers and due to the shear rate, $V_\theta(\theta,\phi = 0)$ [bubble top] $> V_\theta(\theta,\phi = \pi)$ [bubble

bottom]. The term $\partial V_\theta/\partial\phi$ is non-zero and the balance between the various terms induces a non-zero value of V_ϕ and $\partial P/\partial\phi$, contrary to creeping flow where the terms balance properly such that the azimuthal component is zero. At high *Re*, V_ϕ is sought from the pressure field. Taking the divergence of the potential equation of motion, i.e., $-1/\rho\nabla^2 P = \nabla\bullet(\boldsymbol{V}\bullet\nabla\boldsymbol{V})$, and since the r.h.s involves terms like $V_\theta(\theta,\phi)$ and $\partial V_\theta/\partial\phi$, the pressure field is necessarily non-uniform along the azimuthal direction, i.e. the pressure gradient $\partial P/\partial\phi$ appears. Then V_θ results from the balance between the advective terms and the pressure gradient.

NEED FOR LOW GRAVITY

Measurement of the shear lift force on a bubble under normal gravity conditions presents several difficulties. First, the bubble motion is buoyancy driven, and thereby the bubble is constrained by the terminal velocity. Arguments related to counterbalancing the buoyancy force can be made; however, significant deformation of the bubble diameter is expected. Moreover, deformation can cause additional lift because the deformed bubble shape can resemble a hydrodynamic foil, and thus creates the additional lift. This makes the problem more difficult to analyze because the two lifting effects must be separated. The buoyancy force is dominant under normal gravity and masks the other hydrodynamic forces. Low gravity furnishes the proper environment for the other forces to reappear.

EXPERIMENT DESCRIPTION

The experiment consisted of establishing a shear flow in a channel, introducing the bubbles into the flow and dropping the test rig in a 2.2 s drop tower to furnish the microgravity environment. Each of these steps and the associated hardware will be briefly described in this section.

The Flow Channel

The flow channel (2×8×40 cm) was constructed from polycarbonate and fitted with a port for injection of air bubbles into the flow which was established by the Multiphase Flow Rig (MFR) water tank supply. The flow rate of water was measured using a flow meter. The flow was established for 10 to 40 seconds before the air flow was initiated. As bubbles were injected into the channel, the rig was released into the NASA GRC 2.2 drop tower. Observation of the bubble growth and path as it is forming and after detachment was accomplished using a high-speed digital camera running at 500 frames/s. Several diameter injectors were utilized to enable bubble diameter variations. A backlighting approach was used in order to accomplish a high contrast in the high-speed imaging and, in turn, enable the analysis of the bubble motion and the measurement of its diameter. During the drop, the digital imaging data is stored into the camera memory and then downloaded after the drop. Figure 1 shows a schematic of the flow channel geometry and the experimental set up that was integrated into the MFR.

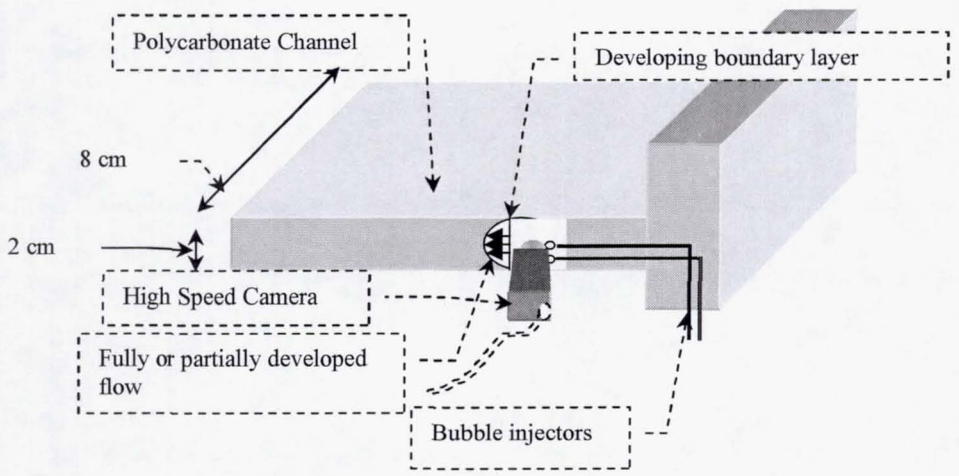

Figure 1. Set up of the shear lift force in a channel flow experiment.

Experimental Parameters

An air-water system was used in these experiments. Table 1 shows the range of experimental parameters that were varied in the low gravity experiments.

Table 1. Summary of the experimental parameters varied in the low gravity experiment.

Parameter [Unit]	Range
Injector D_N [cm]	$0.015 < D_N < 0.158$ cm
Liquid Velocity U_L [cm/s]	$5 < U_L < 9$ cm/s
Gas Flow Rate Qg [cm^3/s]	$0.1 < Q_g < 0.4$ cm^3/s
Bubble Diameter D_B [cm]	$0.2 < D_B < 0.7$ cm
Bubble Re_B Prior to Detachment $Re_B = D_B U_L/\nu$	$170 < Re_B < 650$

EXPERIMENTAL MEASUREMENTS AND UNCERTAINTIES

For each drop, the flow velocity was at first obtained from the liquid flow rate. Using motion analysis software, the bubble diameter, position, velocity and acceleration were measured. The estimated uncertainties in these quantities were used in an error propagation analysis in order to determine the overall uncertainty in the shear lift force. Such an uncertainty was calculated to range between 15 to 29 % of the Shear lift force value, i.e. $0.15 < \Delta F_L/F_L < 0.29$.

RESULTS

Shear vs. Buoyancy Driven Lift

Figure 2 qualitatively shows the difference between the shear (Figure 2(a)) and buoyancy (Figure 2(b)) driven lift acting on a bubble. The frame rate in these two figures is 500 frames/s. It is very clear from the series of images the relative magnitude of the lift on the bubble shape deformation. In the buoyancy driven lift, it can be seen that the bubble is significantly deformed whereas, under microgravity, the bubble retains its spherical shape under shear lift because this force is slight.

Scaling

In order to calculate the shear lift force from the kinematics of the bubble, a force scaling approach was used. As shown in Figure 3, from a simple force balance on the bubble after detachment and before it catches on to the moving fluid velocity, one obtains

$$F_L - F_{Dy} \sim \left(\rho_g + C_M \rho_L\right) V_B y'' \qquad (1)$$

where F_L is the shear lift force, F_{Dy} represents the drag, C_M is the added mass coefficient, V_B is the bubble volume, y'' is the acceleration in the y direction and ρ_g and ρ_L are the gas and liquid densities respectively. The drag force acting on the bubble was determined by

$$F_{Dy} = \frac{1}{2}\rho_L C_D \sqrt{(U_L - x')^2 + y'^2}\, y' \pi \frac{D_B^2}{4} \qquad (2)$$

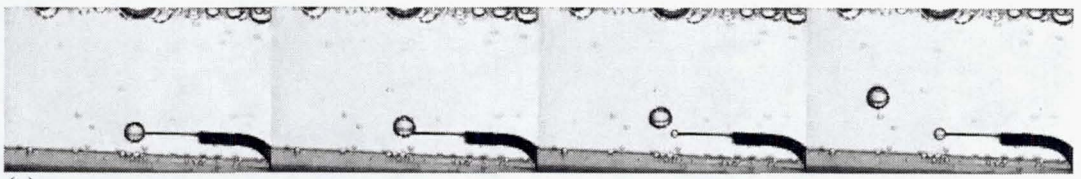

(a)

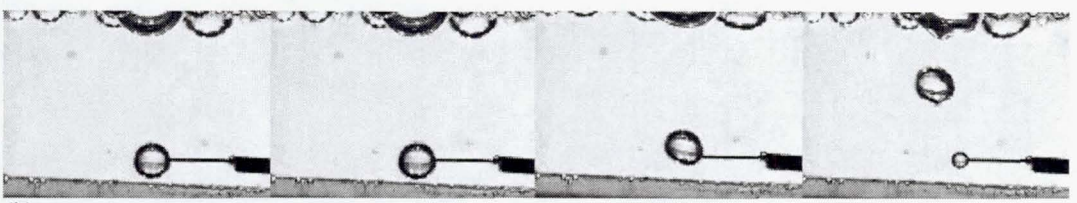

(b)

Figure 2. (a). Shear Lift during the 2.2 s drop. Frames are separated by 80 ms and time moves from left to right. (b). Buoyant lift at the end on the drop. Frames are separated by 40 ms and time moves from left to right.

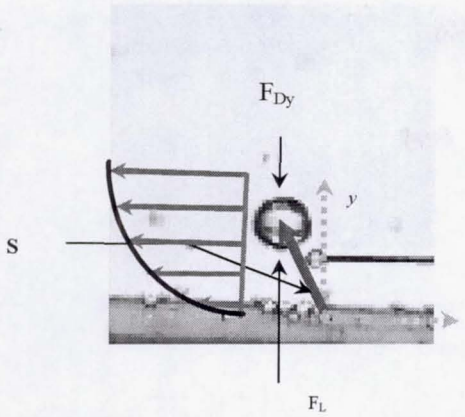

Figure 3. Coordinate system followed in the scaling and trajectory calculation.

In Equation (2), the drag coefficient C_D was derived from the work of Legendre and Magnaudet (1998) who performed a 3-D numerical calculation on the hydrodynamic force on a bubble with a free surface in a shear flow

$$C_D = \frac{15.34}{Re_B} + \frac{2.16}{Re_B^{0.6}} \qquad (3)$$

Here Re_B is the Reynolds number based on the bubble diameter. The bubble volume is calculated from the measured bubble diameter and the bubble acceleration estimated from the rate of change of the velocity with time. The motion analysis software provided the capability of velocity and acceleration measurements. The combination of the above three equations yields the shear lift force. Comparison of the experimentally and theoretically derived lift force is presented in Figure 4, which shows the calculated shear lift force from two models. The first is the Rubinow and Keller, R-K (1961), and the second is Legendre and Magnaudet, L-M (1999). The comparison shows that the agreement is better with the R-K model because the relative velocity is utilized in such a model. In the computation of the shear lift force based on the L-M calculation, the liquid velocity was used instead of the relative velocity. The L-M model is suited for stationary bubble in a shear flow. The bubbles that are under consideration in this study were moving with the fluid and the relative velocity of these bubbles with respect to the fluid is smaller than the fluid velocity.

Trajectory Calculations

Trajectory calculations were performed in order to compare with the trajectories followed by the bubble after detachment. The equations of motion for a bubble moving in a Poiseuille flow were solved for the x and y coordinates as a function of time. The equations of motion for a bubble based on the coordinate system in Figure 3, is given by

$$\sum \bar{F}_B = \left(\rho_g + C_M \rho_L\right) V_B \frac{d^2 \bar{S}}{dt^2} \qquad (4)$$

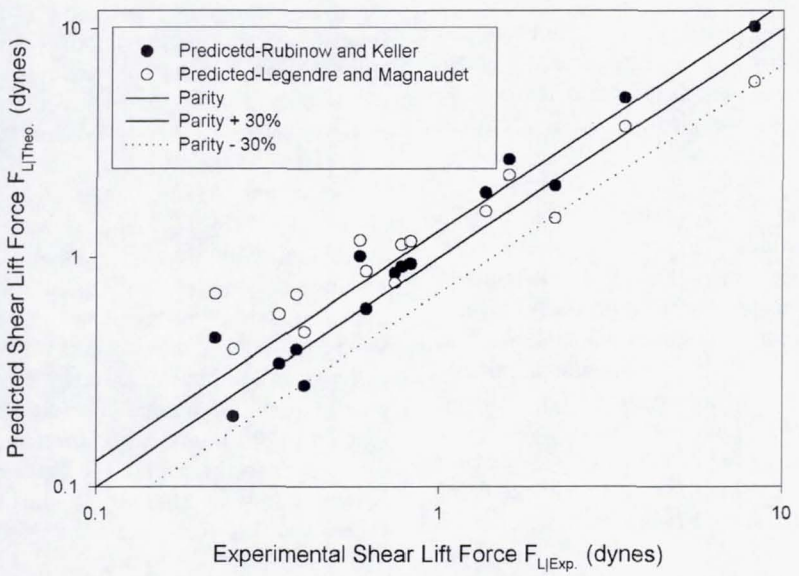

Figure 4. Comparison of the measured and predicted shear lift force. Predictions were based on the Rubinow and Keller and Legendre and Magnaudet's models.

In Equation (4), $\sum \boldsymbol{F}_B$ represents the forces acting on the bubble and the vector $\boldsymbol{S}$ represents the position vector as shown in Figure 3. The x coordinate of Equation (4) results in

$$\left(\rho_g + C_M \rho_L\right) V_B x'' = -\frac{1}{2}\rho_L C_D \left(u_L(y) - x'\right) \times \sqrt{\left(u_L(y) - x'\right)^2 + y'^2}\, \pi \frac{D_B^2}{4} \tag{5}$$

The y direction of Equation (4) results in

$$\left(\rho_g + C_M \rho_L\right) V_B y'' = -\frac{1}{2}\rho_L C_D y' \times \sqrt{\left(u_L(y) - x'\right)^2 + y'^2}\, \pi \frac{D_B^2}{4} + F_L \tag{6}$$

In Equation (5) and (6), D_B is the bubble diameter, x', y', x'', and y'' are the bubble velocity and acceleration in the x and y direction respectively. The initial condition for Equations (5) and (6) are

$$\begin{aligned} x(0) &= x_0, y(0) = y_0 \\ x'(0) &= u_0, y'(0) = v_0 \end{aligned} \tag{7}$$

The initial conditions were obtained experimentally and used in Equation (7). The liquid velocity profile was taken as

$$u_L(y) = 3/2\, U_L\left(1 - y^2/b^2\right) \tag{8}$$

The shear rate of the profile in Equation (8) was calculated accordingly. U_L in Equation (8) is the average flow velocity, which is obtained from the liquid flow rate and the channel cross sectional area.

Figures 5, 6, and 7 show the results of the trajectory calculations. Figure 5 shows the comparison between the measured and calculated bubble trajectory using the Rubinow and Keller model for the shear lift force calculation. The Saffman and Legendre and Magnaudet's models were used for the results presented in Figures 6 and 7 respectively. Table 2 presents a summary of these derived models where the L-M model was derived from the numerical calculation performed by Legendre and Magnaudet (1998).

Table 2. Summary of the shear lift models used in the trajectory calculation.

Model	Expression
Rubinow-Keller	$F_L = \pi \rho_L R_B^3 \bar{\Omega} \times \bar{V}$; $Re_P << 1$
Saffman	$F_L = 6.46\, \rho_L R_B^2 \sqrt{\nu_L\, du_L/dy}\,(u_L - x')$; $Re_P << 1$
Legendre-Magnaudet	$F_L = 1/2\, \rho_L C_L U_r \left(u_L - x'\right)^2 \pi R_B^2$; $C_L^{High\ Re_B} = \left(\frac{1}{2}\right)\frac{1 + 16/Re_B}{1 + 29/Re_B}$; $5 < Re_B < 500$

In Table 2, R_B is the bubble radius, $\boldsymbol{\Omega}$ is the particle angular velocity given by the flow vorticity or $\boldsymbol{\Omega} = 1/2 \nabla \times \boldsymbol{u}$, $\boldsymbol{V}$ is the bubble relative velocity, Re_B and Re_P are the bubble and particle Reynolds numbers based on the liquid velocity and the bubble diameter, U_r is the magnitude of a relative velocity, $U_r = [(u_L - x')^2 + y'^2]^{1/2}$. The Re_B in the C_L equation is expressed as a function of time as well as the shear rate resulting from the velocity profile derivative. The agreement between experiment and trajectories predicted by the R-B and Saffman's model is rather good for the y coordinate in contrary to the trajectory predicted by the L-M model. It is noted that the deviation from experiment occurs at later times in the trajectory predicted with the L-M shear lift. This is because the L-M model is based on a fixed bubble in the shear flow whereas the bubble is moving and the relative velocity of the bubble with respect to the fluid is less than what the model uses. Moreover, as the bubble lifts in the y direction, the shear rate changes, whereas the L-M model used for the calculation of the lift coefficient is independent of the shear rate in the range of Reynolds number shown in Table 2. The reason for the better agreement with the Saffman and R-B models is because the models are suited for low Reynolds numbers, which is the case in the real problem where the bubble quickly catches on the fluid and assumes the liquid velocity. In the L-M numerical computation, the bubble is assumed stationary with respect to the liquid. Therefore, such a model can be applied to the problem of measuring the shear lift on a bubble attached to the injection orifice where the full velocity of the fluid is considered.

It is worth mentioning that the asymptotic solutions and the L-M predictions were based on simple shear, whereas in his work we used Poseuille flow.

The calculation of the low Re_B shear lift coefficient, $C_L^{Low\ Re}$ was described in the numerical study performed by Legendre and Magnaudet (1998). For low Re_B, their derived $C_L^{Low\ Re}$ was given as

$$C_L^{Low\,Re_B} = \frac{6}{\pi^2}\sqrt{Re_B\,Sr}\,\frac{2.255}{\left(1+0.2\varepsilon^{-2}\right)^{3/2}} \qquad (9)$$

In Equation (9), Sr is the dimensionless shear rate given by $Sr = D_B\gamma/U_L$, and ε as $\varepsilon = (Sr/Re_B)^{1/2}$.

For an arbitrary Re_B where $0.1 < Re_B < 500$, they proposed the empirical correlation given by

$$C_L = \sqrt{\left(C_L^{Low\,Re_B}\right)^2 + \left(C_L^{High\,Re_B}\right)^2} \qquad (10)$$

Adoption of this relation into this trajectory calculation results in Figure 8, which shows that the deviation from experimentally measured trajectory is eliminated. The discrepancy in the x coordinate of the bubble trajectory may be due to the uncertainty in knowing the liquid velocity. Measurement of the liquid velocity for various drops/runs using image analysis showed some discrepancy in the velocity as measured from the flow rate and from the software. More investigation of this issue is needed.

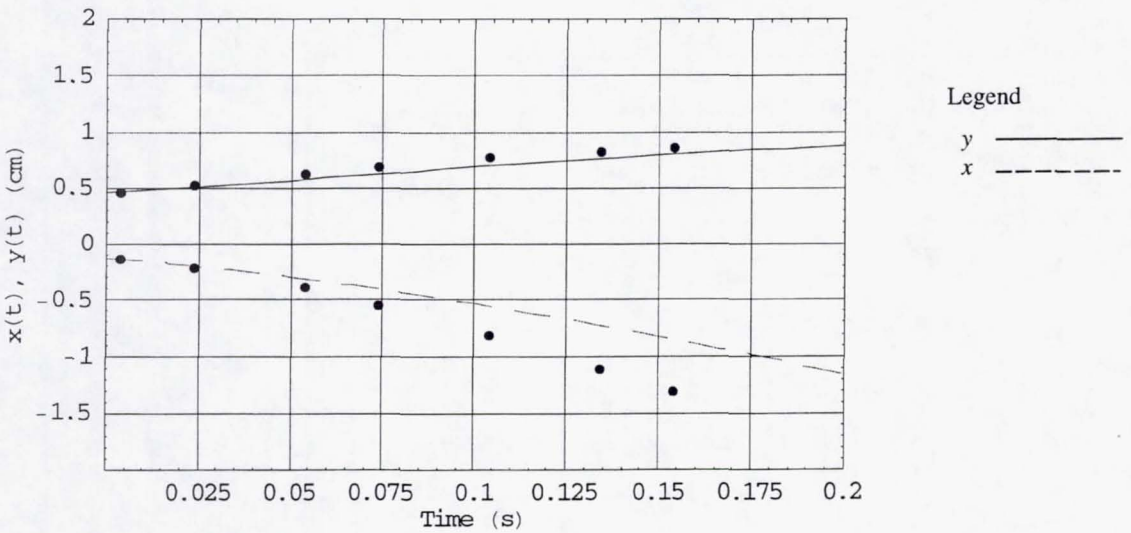

Figure 5. Predicted and experimentally measured bubble trajectory with a shear lift force based on Rubinow and Keller model. $x_0 = 0.12, y_0 = 0.43, u_0 = 2.8, y_0 = 2.0$.

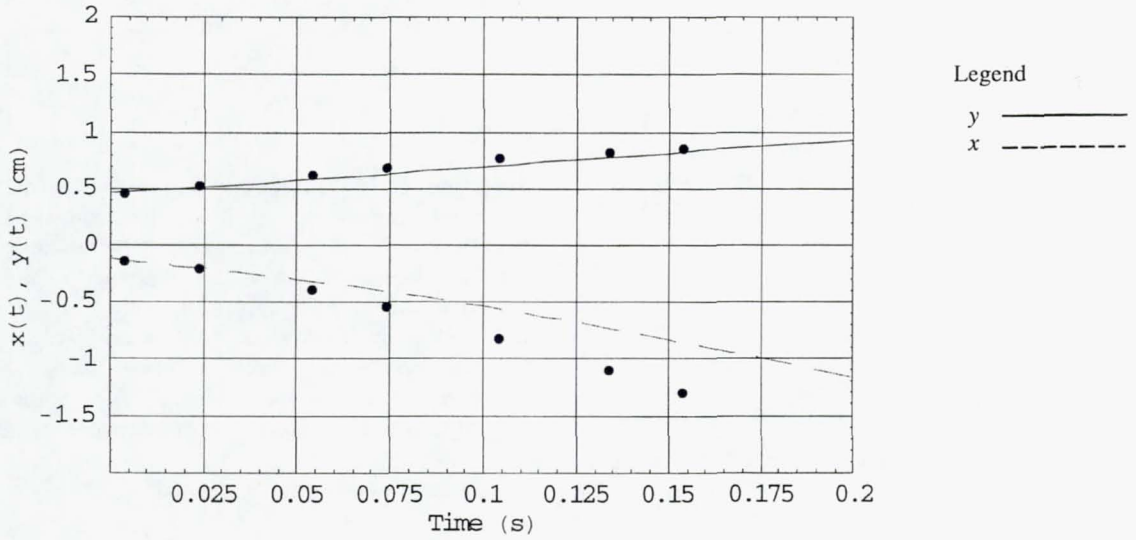

Figure 6. Predicted and experimentally measured bubble trajectory with a shear lift force based on Saffman's model. $x_0 = 0.12$, $y_0 = 0.43$, $u_0 = 2.8$, $y_0 = 2.0$.

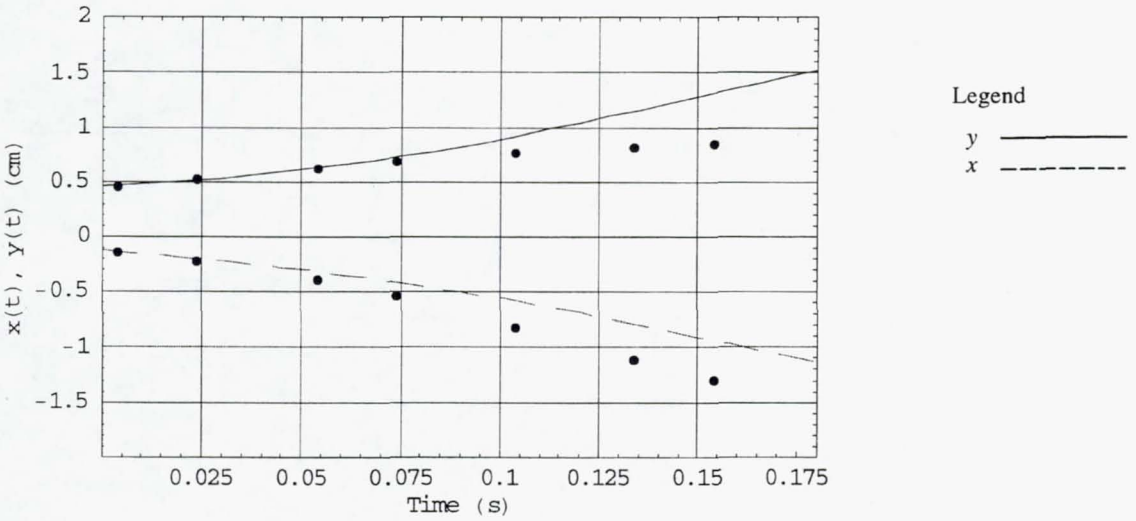

Figure 7. Predicted and experimentally measured bubble trajectory with a shear lift force based on Legendre and Magnaudet's model. $x_0 = 0.12$, $y_0 = 0.43$, $u_0 = 2.8$, $y_0 = 2.0$.

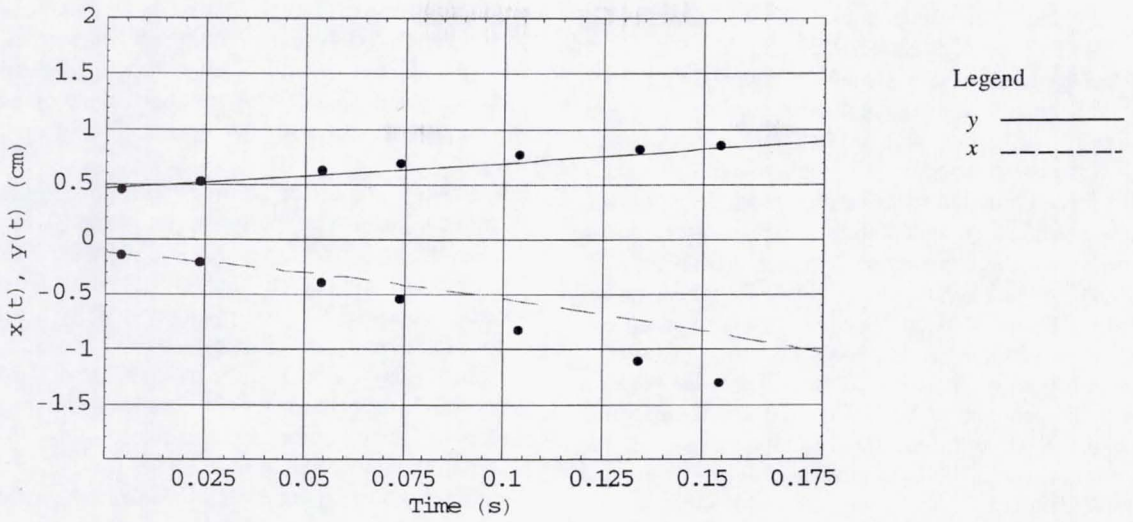

Figure 8. Predicted and experimentally measured bubble trajectory with a shear lift force based on Legendre and Magnaudet's model for the lift coefficient for any Reynolds number. $x_0 = 0.12$, $y_0 = 0.43$, $u_0 = 2.8$, $y_0 = 2.0$.

Comparison with Vasseur and Cox Asymptotic Solution

Cox and Brenner (1968) have obtained a first order expansion in $Re_p = aV/\nu$ of the Navier-Stokes and the continuity equations subject to different boundary conditions on spherical particles, walls, and infinity, from which they obtained the migration velocity. Given the case where a particle of radius a and a distance d from one wall exists between two parallel walls separated by a distance l, their analysis assumed that $Re_p << 1$ and $\kappa = a/l << 1$, and have shown that if $Re_p/\kappa << 1$, that is, if the walls are assumed to be located within the inner region of expansion, one need to consider the inner expansion in order to calculate the first term in the expansion of the migration velocity. It was further shown that if the parameter κ is small, the flow might be calculated by neglecting the size of the particle and assuming that the particle acts as a point force (represented by the delta function) on the flow. Vasseur and Cox (1976) calculated the migration velocity using the expressions derived by Cox and Brenner (1968) for falling particles (non-buoyant and neutrally buoyant) in still fluid near a wall, particles in simple shear and particles in Poiseuille flow. For a neutrally buoyant particle in a parabolic steady flow between two parallel planes, Vasseur and Cox (1976) derived the following expression for the lateral velocity

$$\frac{v_l'}{aU_m^2/\nu\,(a/l)^2} = \frac{256}{3}\pi^3(1-2\beta)\int_{r_3=\beta}^{1}\int_{k_1=-\infty}^{\infty}\int_{k_2=-\infty}^{\infty}\left\{\begin{matrix}\left[(r_3-\beta)-(r_3^2-\beta)\right](4J_3+J_5)+\\(1-2r_3)(4J_4+J_6)\end{matrix}\right\}dk_1dk_2dr_3 = f(\beta)$$

$$\text{for the case where } \kappa^2 >> \left(\frac{V}{U_m}\right) \tag{11}$$

Here β is defined as the ratio of the particle distance to the channel width, d/l, v_l' is the lateral velocity normalized by U_m the velocity that characterizes the flow, V is the particle velocity as caused by the influence of gravity, J_3, J_5, J_4, and J_6 are complicated functions of the k_1 and k_2 in the Fourier Transform domain, and r_3 is the direction of the lateral motion. The integrated result given graphically in the work of Vasseur and Cox was fitted into a polynomial for the ease of evaluation, and used to calculate the theoretical lateral velocity. Several occurrences of smaller bubbles analyzed near the wall were used to compare with the above theoretical results and such a comparison is depicted in Figure 9. The agreement seems reasonable between predicted and measured lateral velocity for these cases of smaller bubbles.

CONCLUDING REMARKS AND FUTURE WORK

Measurement of the shear lift force acting on a bubble in a Poiseuille flow was performed in low gravity using the NASA GRC 2.2 s drop tower. The measurements were compared with the shear lift force predicted from various models. Moreover, basic trajectory calculations were performed in order to indirectly compare model prediction with experiment. The low Reynolds number shear lift formulations (R-B and Saffman models) compared more favorably than high Reynolds numbers-based L-M model reported in Table 2. This was because the real problem at hand reflected the assumptions of the R-B and Saffman models more than the assumptions of the L-M model. However, when the full lift coefficient, which is applicable to any Reynolds number was considered, the agreement between the predicted and measured bubble y coordinate became far better and resembled the agreement with the low Reynolds number models of R-B and Saffman. A comparison of the measured lateral velocity of some smaller bubble analyzed near the wall with the prediction of Vasseur and Cox (1976) was performed as well and showed a reasonable agreement.

Future work is planned to investigate the problem in more controlled experimental settings. Due to the limitation of the liquid reservoir on the MFR, the difficulty of establishing steady flow in the channel, and the more complicated velocity profile within the channel, a couette flow will be used to establish the simple shear. This will be accomplished (as depicted in Figure 10) using a motor-driven belt embedded in a fluid volume. The belt will establish the simple shear flow. Similar experiments will be conducted in simple shear flow and bubble trajectories will be measured in order to calculate the shear lift force. More direct measurements of this lift force are also planned.

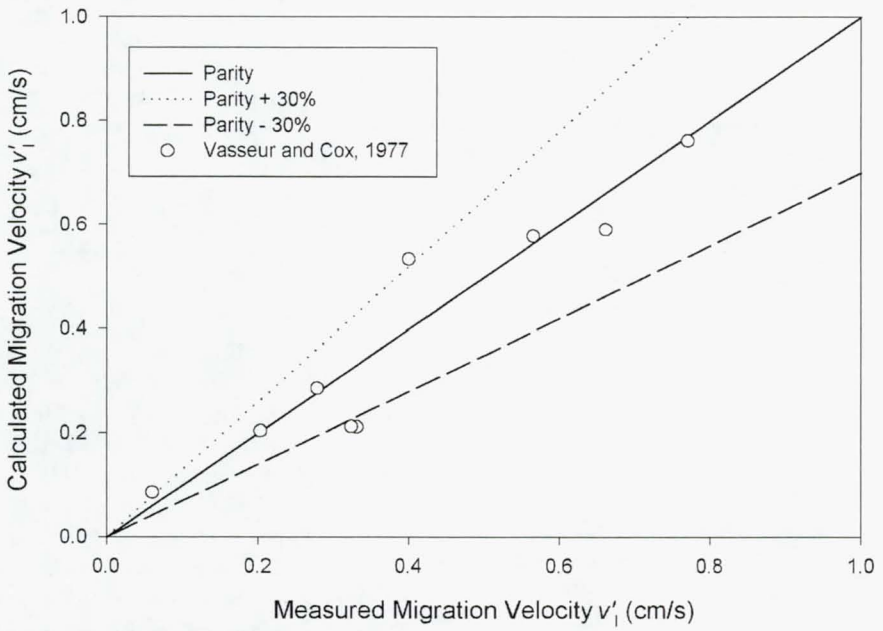

Figure 9. Measured versus predicted lateral velocity of smaller bubbles near the wall.